

Numerical Study of Flow and Pedestrian Level Wind Comfort Inside Uniform and Non-Uniform Street Canyons with Different Street Width to Building Height Aspect Ratios

P. P. Pancholy¹, K. Clemens², P. Geoghegan², M. Jermy², M. Moyers-Gonzalez¹ and P. L. Wilson¹

¹*School of Mathematics and Statistics
University of Canterbury, Christchurch 4800, New Zealand*

²*Department of Mechanical Engineering
University of Canterbury, Christchurch 4800, New Zealand*

Abstract

The aim of this study is to provide input into knowledge-based expert systems by providing mean wind speed at the entire pedestrian level street width. The air flow around an individual building is complex. Around two or more buildings it is even more complicated, a recirculating flow can occur in the street canyon between them. Such urban flows can introduce high wind speeds at pedestrian height inside the street canyon, causing discomfort or even injuries. A fundamental study using the steady Reynolds-Averaged Navier-Stokes (RANS) approach of computational fluid dynamics (CFD) simulations has been performed to analyze the flow pattern and pedestrian comfort inside uniform and non-uniform street canyons for medium rise buildings inside a thick atmospheric boundary layer. For the uniform street canyon study, street width to building height aspect ratios considered (S/H) were 0.5, 0.6, 0.7, 0.8, 0.9 and 1.0 whereas for the non-uniform cases the ratio S/H was kept constant with a value of 1. The Reynolds number involved in this study was 8.1×10^6 based on the height of the building and free stream velocity. This study reveals that for the uniform street canyon cases pedestrian comfort near the downwind building decreases with increasing street width. At $S/H = 1$, the region of approximately 20 – 30% of the width of the canyon at the pedestrian level seating height is in the danger zone for pedestrians. It also reveals that the flow is bistable for the considered range of S/H and for all studied uniform and non-uniform cases. For the step-up street canyon case 100% of the accessible area by pedestrians is in the comfort zone.

Keywords: Atmospheric Research, Atmospheric Boundary Layers, Building Aerodynamics, Pedestrian Comfort

1. Introduction

1.1. Flow structure around and in-between two buildings in tandem arrangement

High rise buildings in urban areas should be designed to ensure comfort of their inhabitants and users. The construction of a building inevitably changes the outdoor environment around the building. These changes include wind speed, wind direction, air pollution, driving rain and heat radiation. The changes in these quantities depend on the shape, size and orientation of the building and on the interaction of the buildings with surrounding buildings [3].

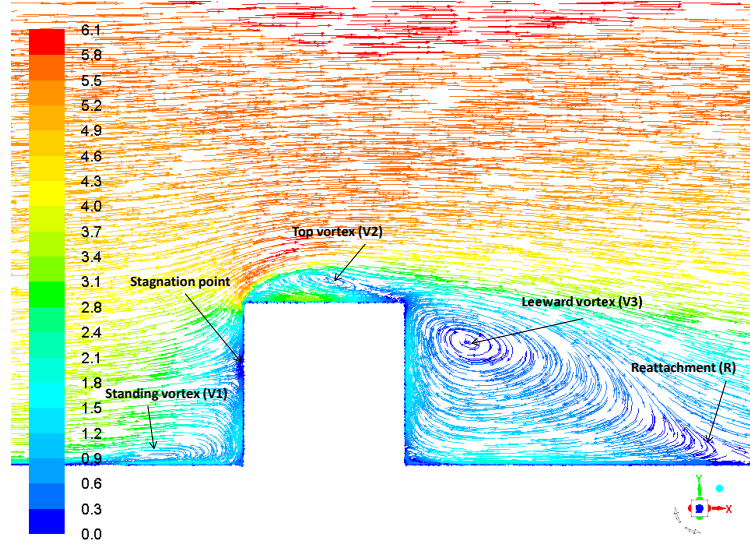
Turbulent flow around a surface-mounted obstacle has long been used as a benchmark problem and studied extensively experimentally to understand the basic flow structure and dynamics of coherent vortex structures around buildings (e.g. Castro and Robins [11]; Martinuzzi and Tropea [28]; Hussein and Martinuzzi [21]; Irtaza et al. [22]; Richards et al. [37]; Sakamoto and Haniu [39] and Larousse et al. [25]). Among the various experiments reported in the literature, Hussein and Martinuzzi [21] performed one of the most detailed experimental measurements and flow visualizations at Reynolds number (Re) of 40,000 based on the obstacle height (H). A number of numerical studies of the flow around a single obstacle have been reported in the literature using steady Reynolds-averaged Navier-Stokes (RANS), unsteady RANS, and large-eddy simulation (LES) turbulence models (e.g. Irtaza et al. [22]; Richards et al. [36]; Yang [46]; Rodi [38]; Shah and Ferziger [41]).

For the general flow features around a surface mounted obstacle as described by Cook [12], when an atmospheric boundary layer (ABL) wind profile approaches normal to the spanwise direction of the obstacle, the wind speed increases with the height above the ground. The flow at about two-thirds of the obstacle height comes to rest to form the front stagnation point. From this point the flow deviates into four main streams. In one of these above the stagnation point, the flow goes up and over the top of the obstacle. Below this point the flow goes down until it reaches the ground where it has more kinetic energy than the incident wind at this level. It is therefore able to move upstream against the wind, losing energy until it comes to rest at a separation point on the ground. The flow rolls up into a horizontal standing vortex next to the ground upstream of the windward face of the obstacle as shown in Figure 1 (a). According to Martinuzzi and Tropea [28], the shape, location and form of the separation region over and in front of the obstacle depends on the boundary layer thickness (δ). The separation point moves closer to the obstacle with decreasing boundary layer thickness.

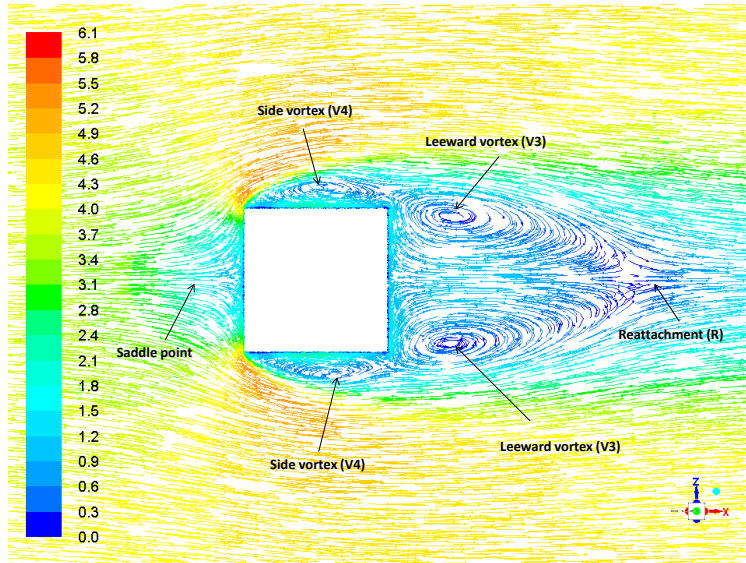
The third and fourth streams are formed by the air entering the standing vortex escaping around either side of the obstacle. When the flow next to the ground is observed, as shown in Figure 1 (b), this vortex forms the shape from which it derives its name of the *horseshoe vortex* [12]. The size and intensity of this horseshoe vortex scales with the thickness δ of the oncoming boundary layer [11]. For thin, laminar boundary layers, (i.e. $\delta/H < 0.3$) the structure of the upstream separation is characterized by multiple secondary recirculations upstream of the horseshoe vortex [40]. Whereas for thicker, turbulent boundary layers (i.e. $\delta/H > 0.7$), the structure of the upstream separation is characterized by a bimodal behavior of the pressure and velocity fields: i.e. the flow in the region between the primary separation and the horseshoe vortex is unstable and fluid in this region is intermittently convected down to the horseshoe vortex [25], [27].

The three streams which separate the from front stagnation point deviate towards the three upstream sharp edges of the obstacle, where they again separate, resulting in strong shear layers, in which turbulence production terms are large [29]. This high turbulence level increases diffusion and enhances entrainment by the shear layer of low momentum reverse flow in the near wake, which strongly affects the local pressure gradient and increases mixing directly behind the obstacle [27]. The horseshoe vortex also entrains the surrounding fluid towards the axis of symmetry. After the reattachment point, an initial rapid expansion of the wake occurs which is due to the increase of the mass flux in the

wake close to the ground as the shear layer reattaches and is subsequently entrained by the horseshoe vortex.



(a)



(b)

Figure 1: Velocity magnitude pathlines (a) passing through the vertical center plane and (b) at ground level (Obtained from the validation study results of this paper for $Re = 6.6 \times 10^4$).

The separated shear layers due to the sharp upstream edges of the obstacle may or may not reattach on the surface of the obstacle. Castro and Robins [11] investigated the influence of δ on the reattachment of these shear layers. According to their observation, if the obstacle streamwise length-to-height ratio (L/H), is sufficiently small relative to δ , the shear layers do not reattach on the obstacle, giving rise to an extended recirculation region in the near wake.

According to Castro and Dianat [10], the streamwise length of the obstacle for which reattachment occurs has been shown to be a function of δ/H .

Reattachment of these separated shear layers is of the utmost importance as it alters the wake flow periodicity which changes the pressure and velocity field near the obstacle. As shown by the Castro [9], the periodicity is a result of the coupled oscillations between the separated shear layers from the lateral sides, which for the surface mounted obstacles, is modified by the shear layer along the obstacle top, the oncoming shear gradient and the appearance of junction or horseshoe vortices. According to their studied case of a thick boundary layer of $\delta/H \approx 6.6$ for the obstacle with spanwise width-to-height ratio $W/H = 1$ and $L/H = 1$, in which reattachment of shear layers occurs on the obstacle surfaces and no periodicity in the wake of the obstacle was observed. Whereas for the studied cases of thick boundary layers by [9] for $\delta/H \approx 1.1$ and by Sakamoto and Haniu [39] for $\delta/H = 0.8$ for taller obstacles with dimension ratio $W/H = L/H = 1/6$ and $W/H = 1/3$ respectively, strong periodicity in the wake was observed.

For multiple obstacle arrays, the flow field is more complex than the flow around a single obstacle due to mutual interference [39]. Experimental studies analyzing the flow structure around a pair of wall-mounted obstacles in tandem have been reported by Meinders and Hanjalić [32] at a low Re of 3854 and for a thin boundary layer; Martinuzzi and Havel [30], Martinuzzi and Havel [31] at a moderate Re of 22,000 and for a thin boundary layer; and Sakamoto and Haniu [39] at a moderately high Re of 1.52×10^5 inside a thick boundary layer. Reported numerical studies on flow around an array of wall mounted cubes include Farhadi and Sedighi [16] and Paik et al. [33] at a moderate Re of 22,000.

Sakamoto et al. [39], have investigated the interference effects of a second obstacle situated in the wake of the first for tall square cross-section, surface mounted obstacles of $W/H = 1/3$. They identified four regimes as a function of gap length (S) as follows: (1) Stable reattachment: when the spacing between the obstacles is in the range of $S/H < 2$, the separated shear layers from both sides of the upstream obstacle attach to the side surfaces of the downstream obstacle and no periodicity is found in the wake. (2) Unstable reattachment or bistable flow: for a larger spacing for $S/H > 2$, a part of the separated shear layers from the upstream obstacle starts to roll up intermittently in to the region between the two obstacles and periodicity is observed in the wake of both obstacles. (3) Stable synchronized: for a critical range of spacing for $S/H \geq 3.5$ separated shear layers roll up strongly in to the gap between the two obstacles without reattachment. (4) Unstable synchronized: for very large spacing of $S/H \geq 50$ between two obstacles the separated shear layers roll up strongly in to the gap between the two obstacles with reattachment.

Martinuzzi and Havel [30] studied the flow around two surface-mounted tandem obstacles of height H , in a thin laminar boundary layer and they found comparatively similar regimes as Sakamoto and Haniu [39], namely (1) a bistable regime for the range $0 < S/H < 1.5$, which is similar to the unstable reattachment regime of [39]; (2) “lock-in” regime for the range $1.5 < S/H < 2.3$ for which case the upstream shear layer impinges on the leading face (near the leading edge) of the downstream obstacle and a strong vortex rolls in the gap and (3) quasi-isolated regime which is similar to the unstable synchronized regime of [39].

The above literature review of the flow past a single and two tandem obstacles suggests that experimental and numerical simulations to analyze the flow structure for two tandem obstacles at very high Re and inside a thick boundary layer have yet to be reported in the literature. This type of flow study is important because generally wind flow around buildings occurs at high Re and inside the thick atmospheric boundary layer. In the present study which has as its aim the study of the flow field between and close to two buildings, we analyze the flow structure around and in-between two medium-rise buildings with equal height and long in spanwise length compared to buildings height, at high Re and for a thick boundary layer in section 3. The impact of changing upstream or downstream building height on the flow structure is analyzed in section 4. Reynolds number based on the height of the building for this study is defined by the equation

$$Re = \frac{\rho \cdot U_{ref} \cdot H}{\mu},$$

where, ρ = air density, U_{ref} = reference wind speed, H = height of the building, and μ = kinematic viscosity of the air.

1.2. Pedestrian comfort inside uniform and non-uniform street canyon

When two or more buildings are lined up along two sides of a street, they create a *street canyon* in-between, which is vertically bounded by the ground surface and the roof level. A street canyon is said to be *uniform* if the adjacent building heights are equal (i.e. $H_1 = H_2$) as shown in Figure 2; and if the adjacent building heights are unequal, it is said to be *non-uniform* (i.e. $H_1 \neq H_2$). In case of the non-uniform street canyon, if $H_1 < H_2$, it is called a *step-up* street canyon and if $H_1 > H_2$, it is called a *step-down* street canyon. The dimensions of a street canyon are expressed by their aspect ratios S/H (street width to building height), and S/W (street width to building width). Note that, in this study the building with the greatest height is used to calculate the aspect ratio.

Urban areas can be characterized as a group of such street canyons. Wind comfort and wind safety for pedestrians are important requirements for urban areas. According to definition of pedestrian comfort by Bottema [8]: “Pedestrian discomfort occurs when wind effects become so strong and occur so frequently (say on time scale up to 1 h), that people experiencing those wind effects will start to feel annoyed, and eventually will act in order to avoid these effects”. This wind comfort and wind safety generally refer to the mechanical effects of wind on people [26]. According to the extended “Land Beaufort scale” of wind effects on people as reported by Lawson et al. [26], at Beaufort Number 3 (gentle breeze or wind speed of 2.4 – 3.8 m/s) these effects include disturbed hair, clothes flapping and newspapers being difficult to read. So, if we consider a person sitting in an open cafe or standing at a bus stop in the street canyon, for example wind can cause disturbance. In this study a reference wind speed of 5.9 m/s was chosen in such a way that we can analyze wind speed according to Beaufort Number 3 at the pedestrian height of approximately 1.75m. This reference wind speed for general CFD and wind tunnel study has been considered as the wind speed at some reference height as representative of the building site. In this study, this reference wind speed has been considered at the building eave height (20 m) (see Appendix for the detailed calculation of the reference wind speed).

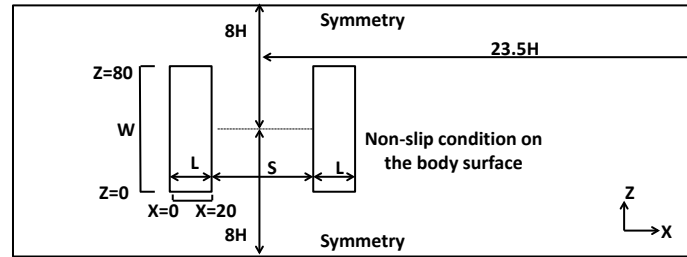
We take our study to be of a fundamental nature, aimed as it is, at a parameteric understanding of the flow field in and around the street canyon. According to Blocken et al. [5], fundamental studies for pedestrian level wind assessment are typically conducted for simple, generic building configurations to obtain insight into the flow behavior, to study the influence of different building dimensions and street widths, to provide input for knowledge-based expert systems (KBES), and for model validation.

Fundamental studies have been conducted by Ishizaki et al. [23] and Wiren [45], who carried out wind tunnel measurements along the street center line between various two-building configurations. Both studies focused on the mean wind speed in the street between rectangular buildings of equal height. Contours of mean wind speed and turbulence measurements at pedestrian level in streets between two high rise buildings of equal height for parallel and perpendicular wind direction using wind-tunnel experiments were provided by To et al. [42]. Numerical studies for two-building models were conducted by Bottema [7] and Baskaran et al. [2]. A very detailed numerical assessment of the influence of varying a wide range of street widths was first conducted by Blocken et al. [5] for parallel wind direction and with buildings of equal height.

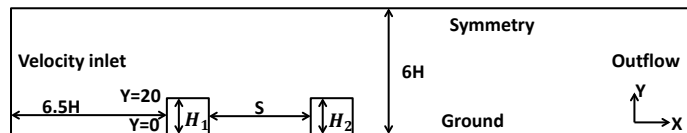
These studies on wind speed conditions in a street canyon were mainly focused on pedestrian-level winds for discrete points, a limited range of street widths and for wind parallel to the street canyon. Detailed CFD study of wind blowing perpendicular to the street canyon still requires more attention. In this study, information using a detailed CFD simulation has been provided for the mean wind speed at the entire pedestrian level street width for the considered wind directions in order to assess pedestrian wind comfort inside street canyons.

2. CFD simulations: computational model and parameters

2.1. Model description



(a)



(b)

Figure 2: Computational domain and boundary conditions for the uniform street canyon (a) Plan view (b) side view.

The model geometry of the uniform street canyon as shown in Figure 2 with dimensions $W \times H \times L = 80(m) \times 20(m) \times 20(m)$ was chosen to represent common medium-rise building structures. The chosen street widths were $S = 10, 12, 14, 16, 18$ and 20 m. These correspond to narrow to regular street width for the medium rise buildings. In the non-uniform street canyon case, the chosen heights of the building were $H_1 = 16$ m and $H_2 = 20$ m for the step-up street canyon, and $H_1 = 20$ m and $H_2 = 16$ m for the step-down street canyon, with a street width of $S = 20$ m for both non-uniform cases.

The effect of changing street width and building heights on the flow pattern and pedestrian wind comfort inside a street canyon was investigated by performing CFD simulations. The size of the computational domain was selected according to CFD best practice guidelines by Franke et al. [17]. The Reynolds number was 8.1×10^6 based on maximum building height and free stream velocity.

2.2. Boundary conditions

Simulations were performed using the commercial CFD package Ansys Fluent version 17.0. The inlet boundary condition was specified according to the recommendations of COST (European Cooperation in the field of Scientific and Technical Research) Action 732 by Franke et al. [17] and using a user defined function (UDF) satisfying Equations 1–4 below for the velocity $U(y)$, turbulent kinetic energy $k(y)$, turbulent dissipation rate $\varepsilon(y)$ and specific dissipation rate $\omega(y)$ respectively:

$$U(y) = \frac{U_{ABL}^*}{\kappa} \ln\left(\frac{y + y_0}{y_0}\right); \quad (1)$$

$$k(y) = \frac{U_{ABL}^{*2}}{\sqrt{C_\mu}}; \quad (2)$$

$$\varepsilon(y) = \frac{U_{ABL}^{*3}}{\kappa(y + y_0)}; \quad (3)$$

$$\omega(y) = \frac{\varepsilon(y)}{C_\mu k(y)}. \quad (4)$$

Here, $\kappa = 0.4$ is the von Kármán constant, y_0 is the aerodynamic roughness length, C_μ is an empirical constant specified in the turbulence model (approximately 0.09) and U_{ABL}^* is the atmospheric boundary layer friction velocity, which can be calculated by a specified velocity U_{ref} at reference height y_{ref} as,

$$U_{ABL}^* = \frac{\kappa U_{ref}}{\ln\left(\frac{y_{ref} + y_0}{y_0}\right)}.$$

Here we take, $U_{ref} = 5.9$ m/s, the free stream wind speed at the building height $y_{ref} = 20$ m to analyze the wind speed between $2.4 - 3.8$ m/s at the pedestrian height.

The top and side boundary conditions were specified as symmetry which is used when expected pattern of the flow solution has mirror symmetry. The outlet boundary condition was specified as outflow, which is used to model flow exits where the details of the flow velocity and pressure are not known prior to solution of the flow problem. The bottom and both building face boundary conditions were specified as wall (no-slip) to bound fluid and solid

regions. Viscous boundary layers were generated on the ground and both building faces with 48 grid layers on each to accurately resolve the boundary layer and accurately predict separation and reattachment points. The height of the first cell of the boundary layer was chosen to be 7.3×10^{-5} m to ensure wall unit $y^+ < 5$ to resolve laminar sub-layer of the boundary layer, which is a requirement of the used turbulent model in this study. The mesh used in this study contains tetrahedral and wedge shaped elements. The boundary layer thickness based on the height of the building was $\delta/H \approx 3.5$, which represents a roughness length $y_0 \approx 0.2$ m and corresponding power law exponent $\alpha = 0.28$ for the real atmospheric boundary layer in which a power-law velocity profile is assumed (see Appendix for the detailed calculation).

2.3. Computational mesh

A mesh independence study was carried out to demonstrate the independence of the flow field on the refinement of the mesh for the flow past a cube with dimension $0.2 \times 0.2 \times 0.2 \text{ m}^3$. The Re was 6.6×10^4 based on the cube height and free stream velocity. The coarse mesh had 1 million cells of resolution 0.01 m on the faces of the cube and 0.02 m throughout the rest of the computational domain. The medium mesh had 2 million cells with resolution of 0.008 m on the faces of the cube and 0.016 m throughout the rest of the computational domain. The fine mesh had 4 million cells and a resolution of 0.006 m on the faces of the cube and 0.012 m elsewhere. The pressure coefficients C_p were measured along the center plane of the cube along the upwind face, the top and the downwind face of the cube.

The main flow features for the coarse mesh are the same as for the fine mesh. Thus, it can be concluded that the coarse mesh is sufficient for running a mesh independent solution. Therefore, in the following work for much larger size buildings the mesh has resolution of 1 m on the faces of the buildings and 2 m throughout the rest of the computational domain. The result is a mesh with approximately 7 million cells.

2.4. Computational model

Different steady RANS models were evaluated, to determine which is best for this study. The cube centerline pressure coefficients C_p for each RANS model were compared with the wind tunnel and CFD study results of Irtaza et al. [22] for the Silsoe cube. The best agreement obtained was approximately 90% in C_p compared to the LES study results of [22] from the transition $k - kl - \omega$ (3 equation model) was obtained.

2.5. Other parameters

The Pressure-Implicit with Splitting of Operators (PISO) algorithm scheme with skewness correction was used for the pressure-velocity coupling as it has a better performance for meshes containing cells with higher than average skewness [22]; pressure interpolation was second-order. Second-order discretization schemes were used for both convective terms and viscous terms of the governing equations. The simulations were initialized by the values of the inlet boundary conditions. Surface monitor points inside the street canyon with (X, Y, Z) coordinates (22, 8, 40), (26, 12, 30), (30, 7, 20), (34, 5, 70), and (38, 10, 50) were used to measure convergence. These are the points used for

$S/H = 1$ and are changed accordingly with change in aspect ratio S/H . The simulations were terminated when all specified surface monitor points reached the criteria of a difference in value between two iterations of 0.0005 for 20 consecutive iterations. Incompressible flow with the air density $\rho = 1.225 \text{ kg/m}^3$ was used in this study. The kinematic viscosity of the air considered in this study was $\mu = 1.7894 \times 10^{-5} \text{ kg/m} \cdot \text{s}$.

2.6. Validation

Vardoulakis et al. [43] and Ratnam et al. [34] reported that the most widely studied flow problem in wind engineering is a 3D cube immersed in a turbulent boundary layer due to the simplicity of the shape and the complexity of the flow around the cube. Therefore, validation of the CFD model was performed by first simulating the wind flow around a surface mounted cube in a turbulent channel flow. In this study, the pressure coefficients C_p along the vertical centerline of the windward face, the roof and the leeward face were compared with the wind tunnel and CFD study results of Irtaza et al. [22] for the Silsoe cube. Here, C_p is defined by the equation

$$C_p = \frac{P_{static} - P_{ref}}{\frac{1}{2}\rho_{ref}U_{ref}^2},$$

where, P_{static} is the surface static pressure, P_{ref} is the reference pressure, and ρ_{ref} is the air density.

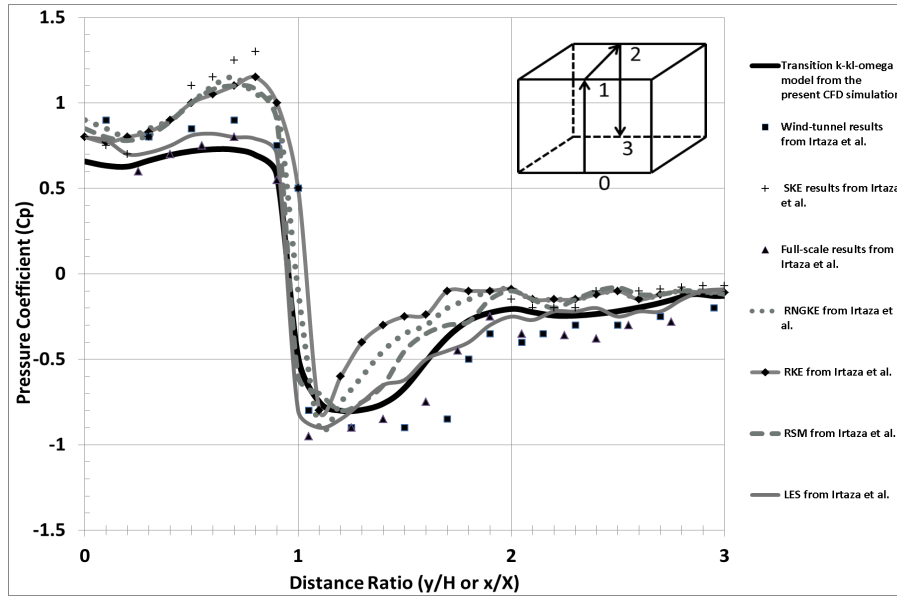


Figure 3: Pressure coefficient comparison plot along the center plane of cube.

In order to assess the accuracy of the CFD simulation results, the pressure distribution along the vertical centerline of the windward face, the roof and the leeward face were investigated. The location of the maximum positive pressure coefficient $C_p = 0.73$ where stagnation occurs on the windward face of the cube, occurred at a distance of $0.6H$ from the ground. On the roof the maximum negative pressure $C_p = -0.80$ was observed at a distance of $0.2H$ from the

windward edge of the roof. For the downwind face the maximum negative pressure $C_p = -0.24$ occurred at location $0.7 H$ from the ground. Obtained values of the pressure coefficient were compared with the CFD simulations, wind tunnel test and full-scale study results of Irtaza et al. [22] as shown in figure 3, and with previously published in-situ measurements, wind tunnel tests and validated CFD simulations as shown in Table 1, and summarized below.

	Location of the maximum positive C_p on the front of the cube from the ground	Location of the maximum negative C_p on the roof of the cube from the windward edge	Location of the maximum negative C_p on the back of the cube from the ground
Transition $k - \epsilon - \omega$ used in this study	0.73 at 0.6 H	-0.80 at 0.2 H	-0.24 at 0.7 H
Irtaza et al. [22] Standard $k - \epsilon$	1.3 at 0.8 H	-0.8 at 0.1 H	-0.2 at 0.9 H
Irtaza et al. [22] RNG $k - \epsilon$	1.15 at 0.7 H	-0.9 at 0.1 H	-0.15 at 0.9 H
Irtaza et al. [22] Realizable $k - \epsilon$	1.15 at 0.8 H	-0.8 at 0.1 H	-0.15 at 0.8 H
Irtaza et al. [22] RSM	1.1 at 0.7 H	-0.8 at 0.1 H	-0.2 at 0.2 H
Irtaza et al. [22] LES	0.82 at 0.6 H	-0.9 at 0.1 H	-0.27 at 0.9 H
Richards et al. [36] (CFD)	0.81 at 0.8 H	-0.97 at 0.05 H	-0.17 at 0.85 H
Yang [46](CFD) CFX5 $k - \epsilon$	0.95 at 0.82 H	-1.56 at 0.05 H	-0.3 at 0.76 H
Yang [46](CFD) CFX5 RNG $k - \epsilon$	0.9 at 0.8 H	-0.85 at 0.05 H	-0.4 at 0.81 H
Irtaza et al. [22] Wind tunnel	0.9 at 0.7 H	-0.9 at 0.25 H	-0.4 at 0.95 H
Castro and Robins [11] Wind-tunnel	0.78 at 0.85 H	-0.9 at 0.1 H	-0.1 at 1 H
Hölscher and Niemann [20] (Average of 15 wind tunnel)	0.87 at 0.75 H	-1 at 0.27 H	-0.2 at 1 H
Richards et al. [37] Wind tunnel	0.75 at 0.81 H	-1.1 at 0.2 H	-0.2 at 1 H
Irtaza et al. [22] Full scale	0.8 at 0.7 H	-0.95 at 0.05 H	-0.38 at 0.4 H
Richards and Hoxey [35] In-situ	0.86 at 0.81 H	-0.9 at 0.15 H	-0.1 at 1 H

Table 1: Comparison of obtained pressure coefficient results with published results of in-situ measurements, wind tunnel tests and CFD simulations.

Values of C_p lie within the range of previously obtained results. The stagnation point occurred at 0.6 H , which is similar to LES results of Irtaza et al. [22], and the obtained C_p value of 0.73 at this point is close to the value observed in the wind tunnel study of Richards et al. [37] and Castro and Robins [11].

On the roof of the cube, the maximum negative pressure coefficient value occurs at a distance of 0.2 H , which is similar to the wind tunnel results of Richards et al. [37], Hölscher and Niemann [20] and Irtaza et al. [22]. The value of the C_p is -0.8, which is similar to the CFD simulation (Standard $k - \epsilon$ model, Realizable $k - \epsilon$ model and RSM model) results of Irtaza et al. [22], as well as the CFD simulation results of Yang [46].

On the downwind face, the maximum negative C_p occurred at a distance of 0.7 H , which is close to the results of

the CFD study by Yang [46] (CFX5 $k - \epsilon$), while the value $C_p = -0.24$, is close to the LES results of Irtaza et al. [22] and to the wind tunnel study results of Hölscher and Niemann [20] and Richards et al. [37].

From Figure 3 it could be concluded that none of the CFD study results of Irtaza et al. [22] matches well with their experimental data, but their LES is the best match and the obtained results from the present study matches well with their LES results which gives more confidence in the simulation variables used.

From the above listed literature review on previous CFD studies in Table 1 and from the present study comparison plot Figure 3, variation between studied results is observed. The reasons for these discrepancies may be due to variation in mesh elements, degree of convergence, turbulence model, the flow Re and perhaps also the intrinsic stability of the flow field behind a bluff object.

3. Results and discussion for the uniform street canyon

3.1. Flow structure around and inside the uniform street canyon

Results of flow simulation for a uniform street canyon with different street-to-height ratios S/H of 0.5, 0.6, 0.7, 0.8, 0.9 and 1.0 are presented in this section. Figure 4 and 5 show the variation of C_p along the center plane ($Z = 40$) for different uniform street canyons on the ground from the inlet of the flow up to the upstream building, and for the different faces of the upwind building respectively.

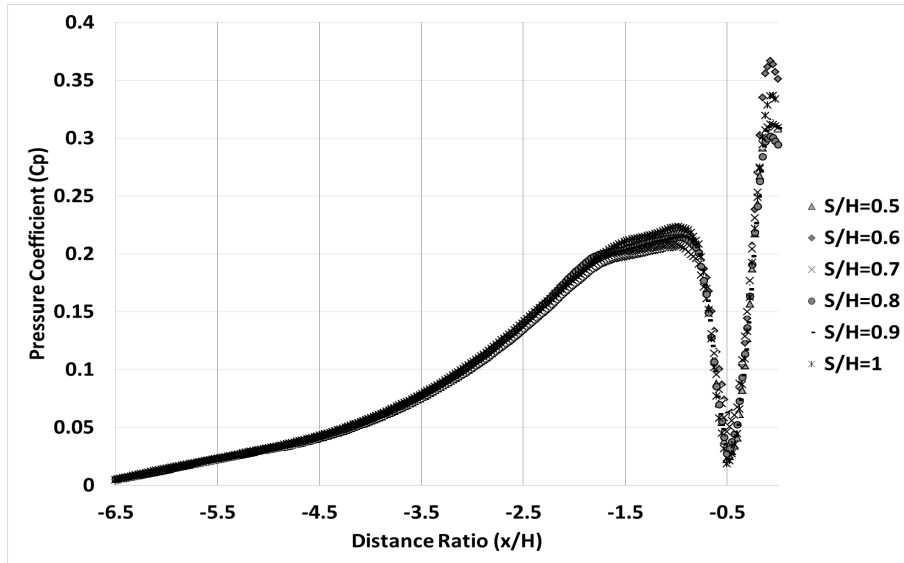


Figure 4: Pressure coefficient comparison plot on the ground upstream of the upwind building along the center plane for the considered uniform street canyon cases.

From Figure 4 it can be observed that inside the thick boundary layer ($\delta/H \approx 3.5$ in the present study) the change in far upstream values of C_p is nearly equal for the different studied cases. The pressure minimum near the upstream building is located near the horseshoe vortex at around $0.5 H$ upstream of the windward face. In addition, the pressure

maximum at around $0.9H$ corresponds to the location of the upstream stagnation point which causes an increase in the surface pressure. The location of the horseshoe vortex and stagnation point for the different studied cases are identical but differences in the value of C_p are observed. The reason for these differences may be due to the unstable behavior of the flow in this region as described by Larousse et al. [25].

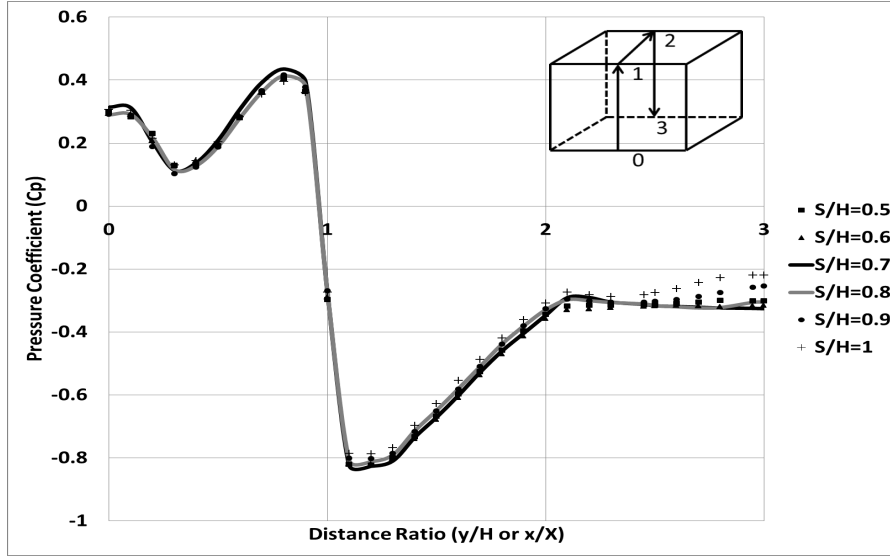
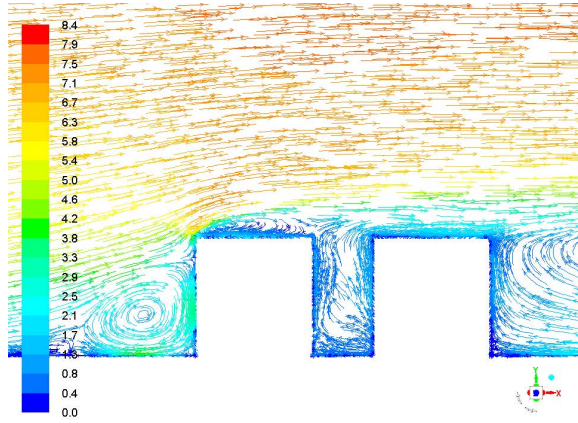
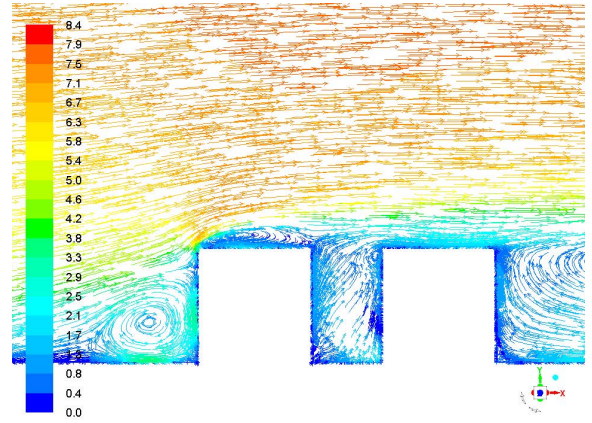


Figure 5: Pressure coefficient comparison plot along the center plane of the upwind building for the considered uniform street canyon cases.

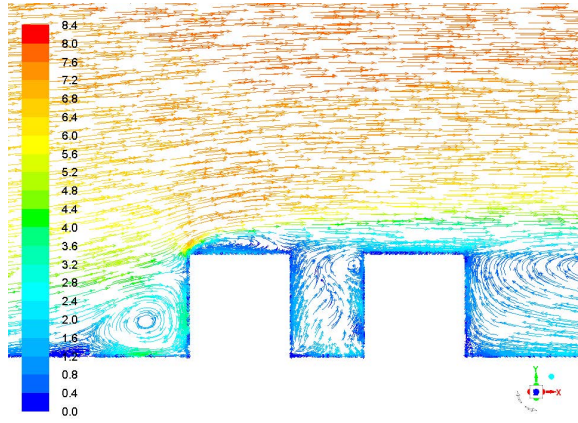
From Figure 5 it is observed that the stagnation point on the front face of the upstream building occurs at about $0.8H$ from the ground for all studied cases. From this point the flow diverts into four different streams as described in section 1.1. The point of minimum positive C_p which is identical for all studied cases occurs on the front face at about $0.4H$ above the ground. The stream which deviates toward the roof again separates due to the front sharp edge and the separated shear layer reattaches on the same roof surface and bifurcates. This flow structure can be clearly observed in Figure 6 and detailed view of the same in Figure 7(b). According to Castro and Robins [11], at the leading edge of the upstream building roof, separation causes a high negative pressure which indicates the minimum C_p region. This pressure increases toward the trailing edge and recovers to nearly zero pressure which suggests that the flow may reattach on the top surface. Also, they specified from their analysis that for $\delta/H > 0.7$ the separated shear layer permanently reattaches on the top of the building which explains the reattachment of the shear layer on the same surfaces for our studied cases for $\delta/H \approx 3.5$. The negative pressure on the rear face of the upstream building varies due to strong mixing of the fluid in the street canyon with that from entrainment [39].



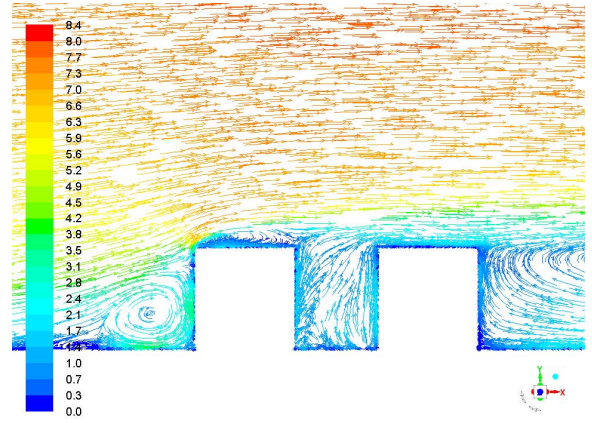
(a) $S/H = 0.5$



(b) $S/H = 0.6$



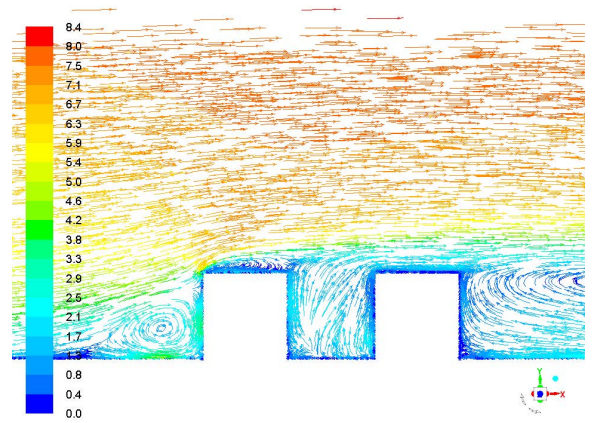
(c) $S/H = 0.7$



(d) $S/H = 0.8$



(e) $S/H = 0.9$



(f) $S/H = 1$

Figure 6: Velocity magnitude (m/s) pathlines in XY -plane at the center plane ($Z = 40$) for the uniform street canyon with different street aspect ratios.

The separated flow on the roof of the upwind building gives rise to a large three-dimensional recirculation region over the roof as can be seen in Figure 6 and closer inspection of the same in Figure 7(b), in which the vortex core can be recognized at approximately $0.25H$ downstream of the leading edge. Most of the flow from the roof of the upwind building diverts towards the roof of the downwind building. Back-flow from the canyon is forced into the roof region of the upwind building resulting in a secondary recirculation at the trailing edge of the upwind building roof. By reason of continuity along the plane of symmetry, the back flow is forced laterally to be re-entrained by the main flow [15]. The flow in the canyon for different S/H ratio can be characterized by a strong fluid stream directed upwards and towards the windward face of the downwind building. A small recirculation can be observed in the case of $S/H = 0.6$ and 0.7 near the top corner of the windward wall of the downwind building.

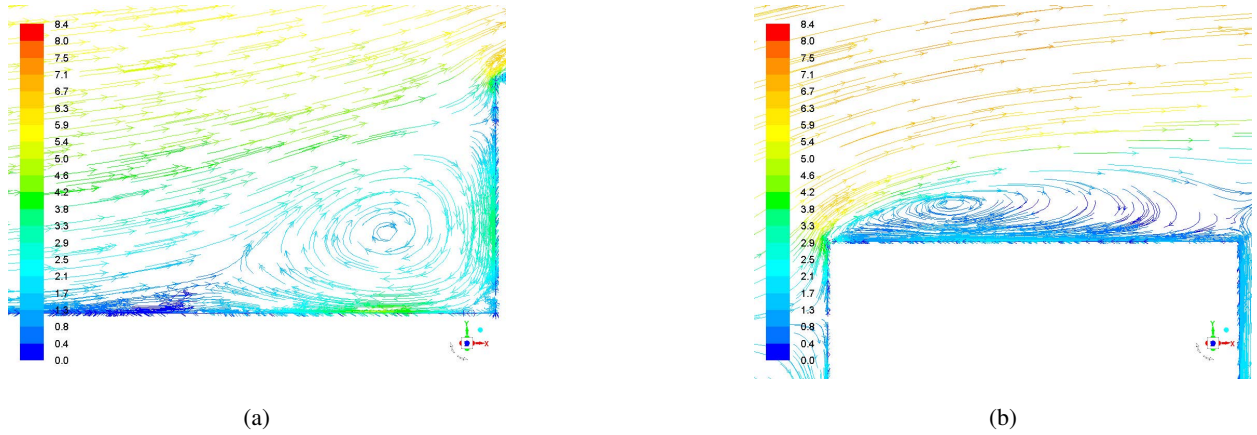


Figure 7: Detailed view of (a) the flow structure upstream of the upwind building and (b) the flow separation on the roof of the upwind building using velocity magnitude (m/s) pathlines in XY - plane at center plane ($Z = 40$) for street canyon with aspect ratio $S/H = 1$.

Figure 7(a) represents a closer view of the upstream separation region for $S/H = 1$, which reveals that the horseshoe vortex system actually consists of a complex vortex structure. The extension of the horseshoe vortex along the sides of the uniform street canyon can be seen in the velocity magnitude pathlines plot in Figure 8. On the side faces of the upwind building, separated flow at the leading edges give rise to intense corner vortices. For these separated shear layers, reattachment occurs inside the canyon gap even at the smallest canyon length $S/H = 0.5$. This is probably due to the combined effect of the horseshoe vortex and solid walls of the building as explained by Havel [19]. Thus the horseshoe vortex tends to convect the fluid towards the buildings and inside the canyon. Whereas the fluid entering into the canyon due to the flapping of the roof shear layer from the upwind building ([19]) exits to the sides. This interaction confines the lateral shear layers and pushes them outward, which allows the development of the second vortex street inside the canyon.

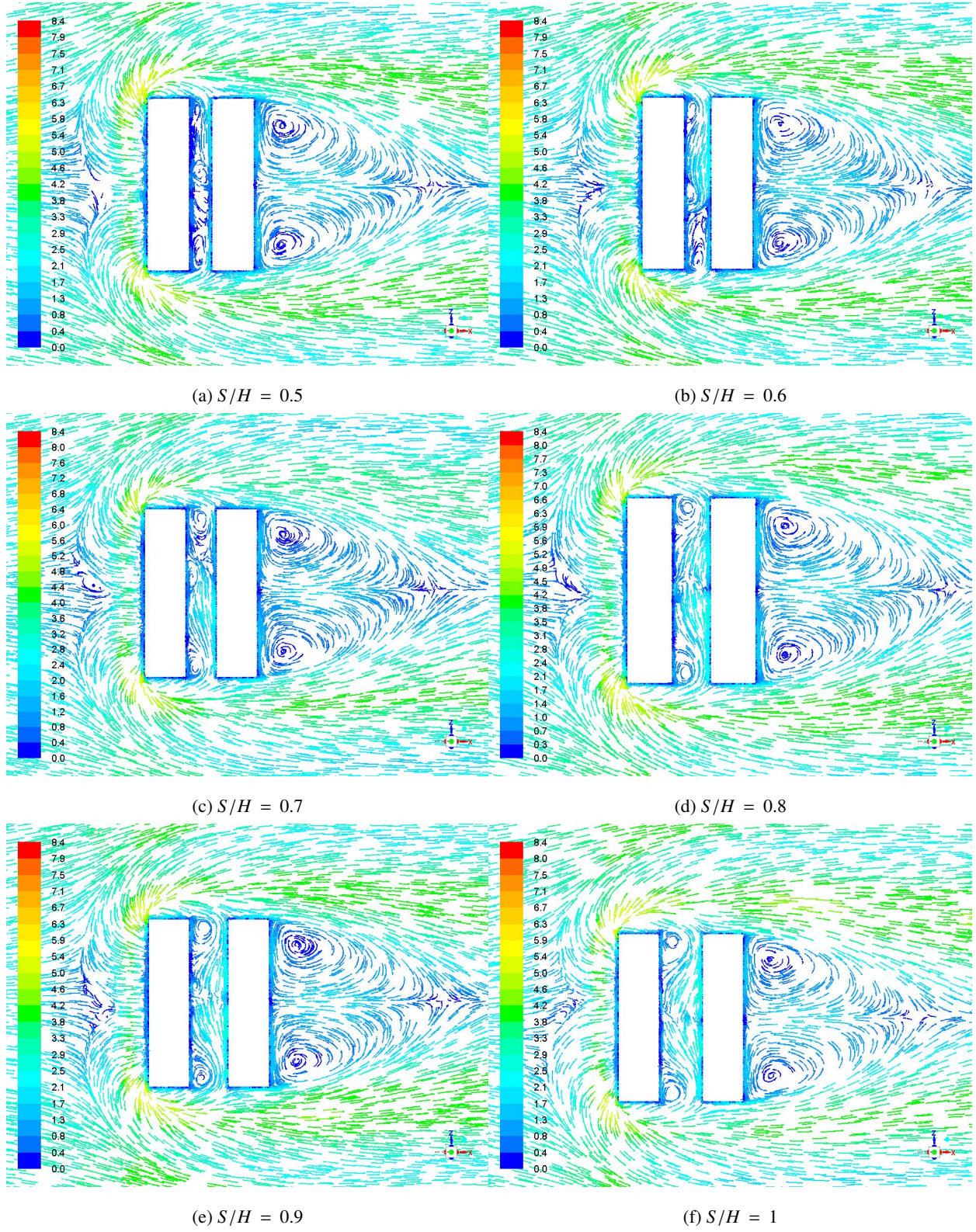


Figure 8: Velocity magnitude (m/s) pathlines in XZ - plane at $Y = 1$ m level for the uniform street canyon with different street aspect ratio.

Figure 8 represents the velocity magnitude pathlines near the ground level to show the complex flow structure at the ground level for different uniform street canyons. Since the flow between horseshoe vortex and upstream stagnation point is unstable, velocity takes one of the two preferred states. Which indicates the bimodal form of the distribution as explained by Larousse et al. [25].

From the above flow visualization of the flow separation from the leading edges of the upwind building, it can be generalized that the separated shear layer from the roof of the building reattaches on the same roof surface whereas separated shear layers from the lateral surfaces reattach inside the canyon gap. For this kind of flow behavior Havel [19] has revealed that when the shear layer does not reattach on the sides of the second building, low frequency vortex shedding can be observed inside the canyon. Whereas, if the shear does reattach on the second building, vortex shedding would be induced downstream of the second building, which results in the high frequency. This type of bistable flow behavior where the low frequency vortex shedding occurs inside the canyon gap can be predicted in these studied cases.

Figure 9 shows the view of the coherent vortex structure over the first building, in the gap between buildings, and over the top of the second building observed from the pedestrian level height. The shear layer reattachment on the top of the upwind building can be clearly seen in this image.

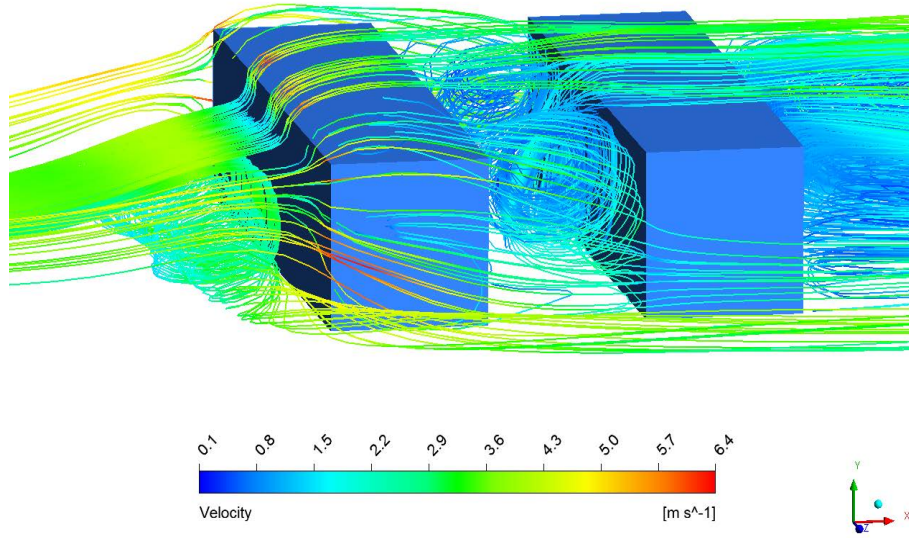


Figure 9: Isometric view of streamlines showing coherent vortex structure around and inside the uniform street canyon for $S/H = 1$.

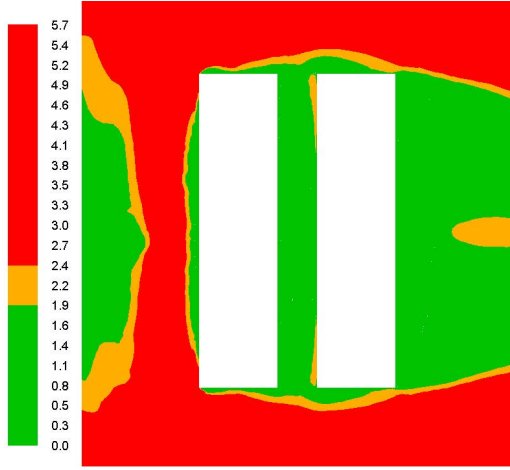
3.2. Pedestrian comfort inside the uniform street canyon

Figure 10 shows contour plots of pedestrian comfort at a height of 1 m inside the street canyon for the different uniform street canyon cases considered in this study. This height can generally be considered as the seating height of a person. As street width increases, the wind speed inside the street canyon near the upwind wall of the downwind

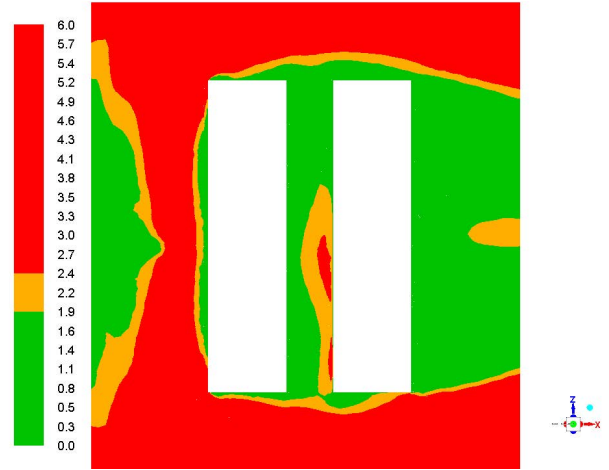
building increases. Almost 100% area near any point on the downwind wall of the upwind building which could be in frequent use by pedestrians is in the comfort zone. In case of $S/H = 0.5$, only a small region of approximately 2 m in the streamwise direction and approximately 10 m near the corners or in the spanwise direction near the downwind building is uncomfortable for pedestrians (i.e. wind speed between $1.81 - 2.4\text{ m/s}$, according to extended “Land Beaufort Scale” by [26], which represents wind speed in the range of Beaufort Number 2 and 3). For $S/H = 0.6$, a region of approximately 2 m in the streamwise direction and from $Z = 0$ to $Z = 50\text{ m}$ near the downwind building can be found as a danger zone (i.e. wind speed above 2.4 m/s) for pedestrians. In the cases of $S/H = 0.7, 0.8, 0.9$ and 1.0 , approximately 5 m^2 near the center part of the downwind building can be seen as a comfortable zone for pedestrians. In the cases of $S/H = 0.9$ and $S/H = 1$, most of the area near the downwind building inside the street canyon is in the danger zone for pedestrians.

Figure 11 shows contour plots of pedestrian comfort at a height of 1.75 m inside the street canyon for different uniform street canyon cases considered in this study. This height can generally be considered as the average head height for pedestrians. At this height an overall reduction in the wind speed can be observed compared to the case of pedestrian seating height. This is due to the reason that the significant downflow of air at the windward face from the front stagnation point that subsequently enters into the canyon from the ground level. It is also explained by Blocken et al. [5] that very pronounced increase of wind speed in the canyon is limited to the near ground level and decreases with increase in height in the y -direction. They give the reasons that: (1) the pressure gradient is more pronounced near the ground level and (2) there is a considerable amount of air leaving the canyon through the top plane. As street width increases, the wind speed near the upwind wall of the downwind building increases. Most of the area near the upwind wall of the downwind building which was in the danger zone at seating height can now be observed to be in the discomfort zone at this height. An area of danger can be found near the corners of the leeward wall for the downwind building in the case of $S/H = 0.9$ and $S/H = 1$.

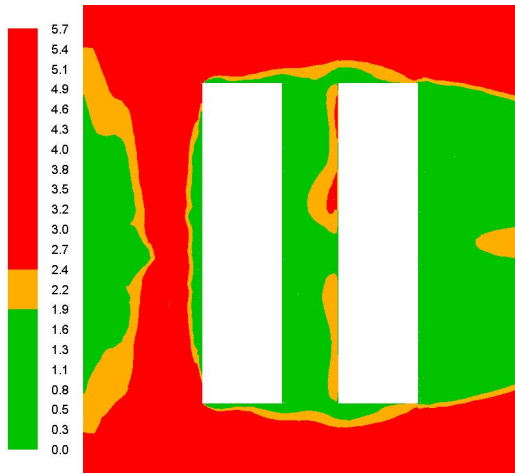
From the above pedestrian comfort assessment study for different uniform street canyons it can be seen that the overall wind velocity near the downwind building area which would be in frequent use by pedestrians increases with increase in the ratio S/H . Overall reduction in the wind speed has been observed with the increase in height in the y -direction which converts the danger zones into discomfort zones for pedestrians. There is no significant increase in the wind speed near the downwind wall of the upwind building near the pedestrian accessible zone has been observed.



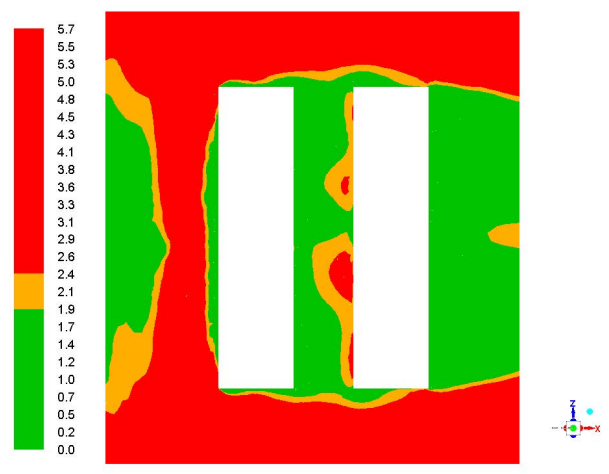
(a) $S/H = 0.5$



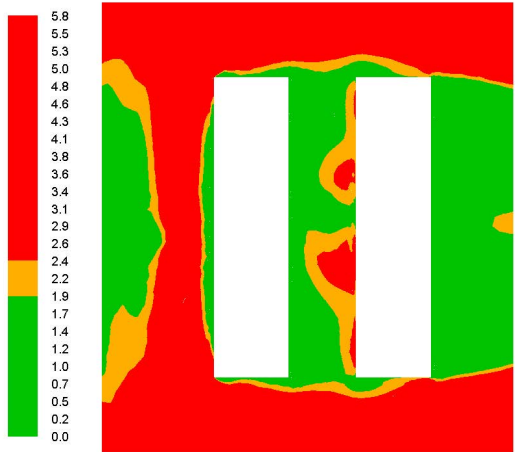
(b) $S/H = 0.6$



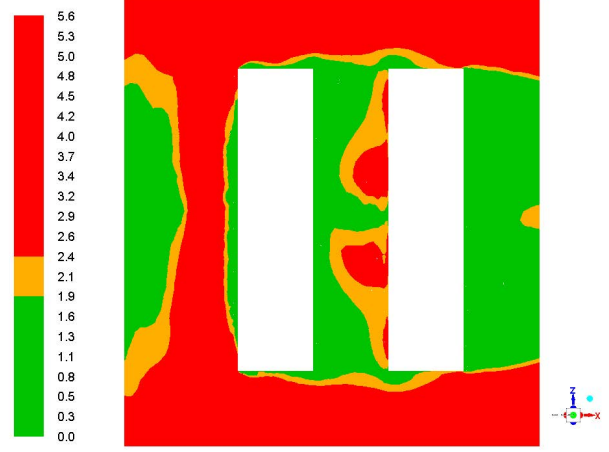
(c) $S/H = 0.7$



(d) $S/H = 0.8$

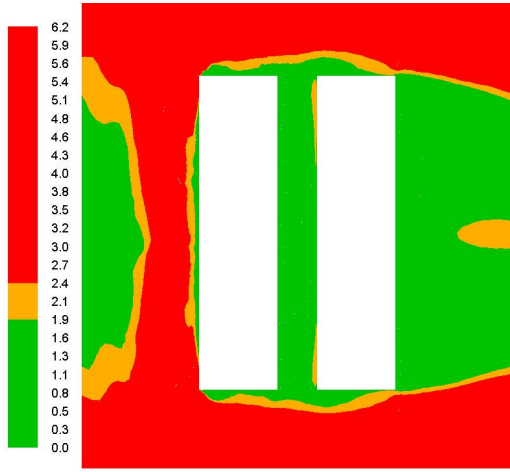


(e) $S/H = 0.9$

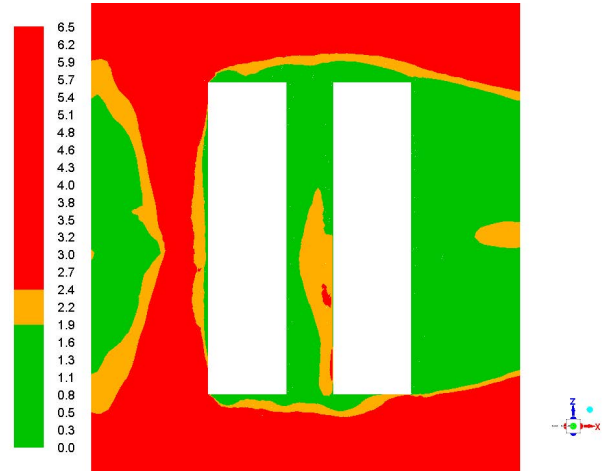


(f) $S/H = 1$

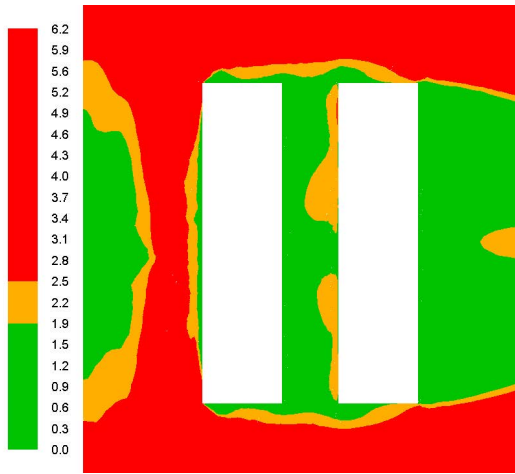
Figure 10: Velocity magnitude (m/s) contours at $Y = 1$ m in the XZ- plane for the uniform street canyon with different street aspect ratio. Here, green represents 0 to 1.8 m/s (which can be considered a comfort zone for pedestrians), orange represents 1.81 to 2.4 m/s (zone in which the wind starts causing impact on people), red represents wind speeds above 2.4 m/s (the danger zone).



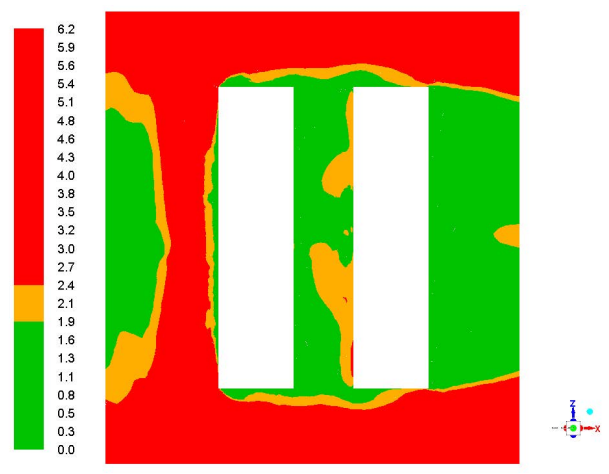
(a) $S/H = 0.5$



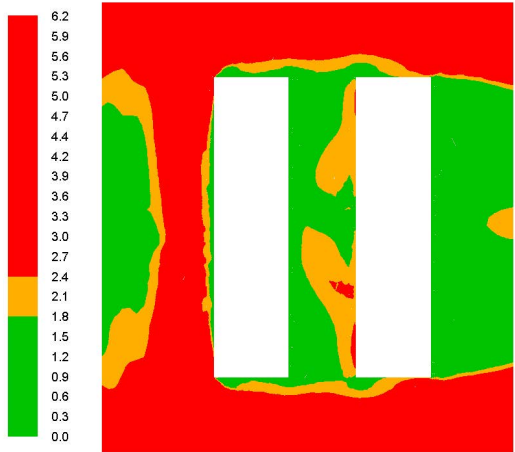
(b) $S/H = 0.6$



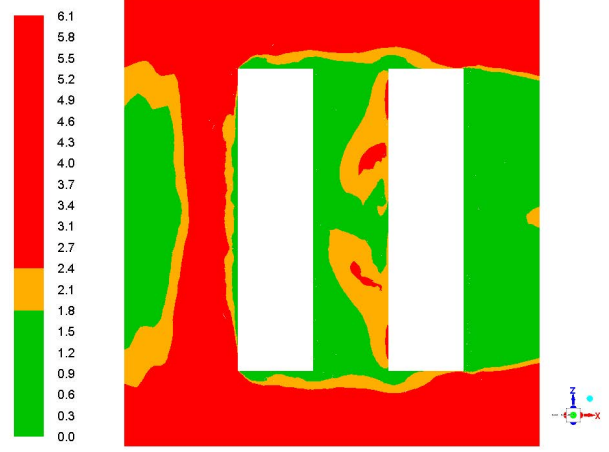
(c) $S/H = 0.7$



(d) $S/H = 0.8$



(e) $S/H = 0.9$



(f) $S/H = 1$

Figure 11: Velocity magnitude (m/s) contours at $Y = 1.75$ m in the XZ- plane for the uniform street canyon with different street aspect ratio. Here, green represents 0 to 1.8 m/s (which can be considered a comfort zone for pedestrians), orange represents 1.81 to 2.4 m/s (zone in which the wind starts causing impact on people), red represents wind speeds above 2.4 m/s (the danger zone).

4. Results and discussion for non-uniform street canyon

4.1. Flow structure around and inside the non-uniform street canyon

To analyze the impact of changing the height of the upwind building or the downwind building on the wind speed and pedestrian comfort inside the street canyon, simulations have been carried out for step-up and step-down street canyons and compared with the uniform street canyon studied case of $S/H = 1$. Most of the flow characteristics for both studied non-uniform cases are similar to that discussed in section 3.1 for the uniform street canyon. These common features include flow separation on the ground before the upwind building, generation of the horseshoe vortex, stagnation point on the front face of the upwind building, separation of the flow from the leading edges of the upwind building and reattachment of the separated shear layer from the roof of the upwind building on the same surface.

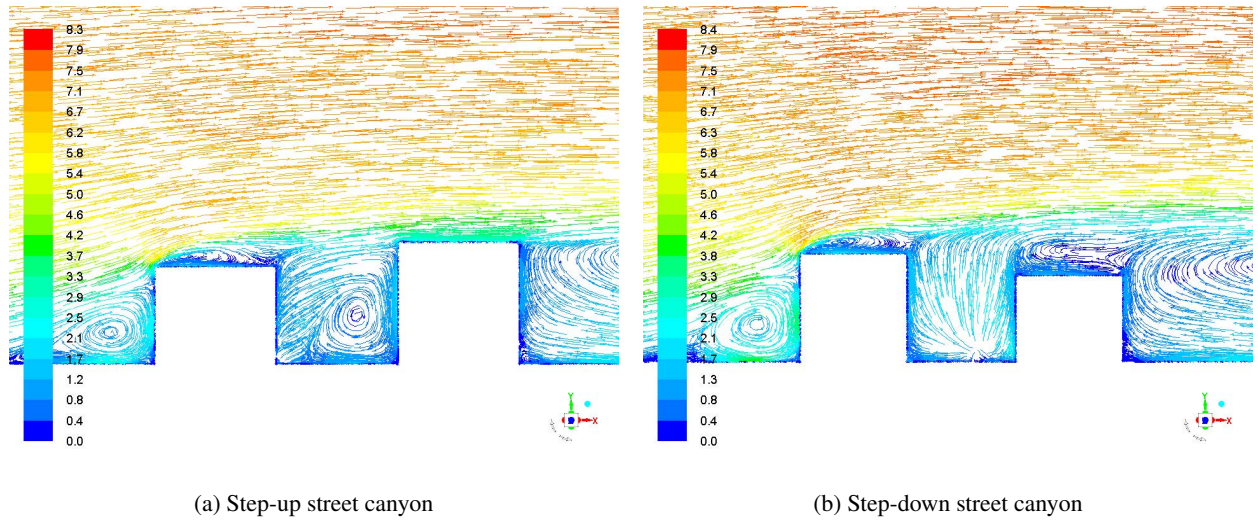


Figure 12: Velocity magnitude (m/s) pathlines in XY -plane at center plane ($Z = 40$) for the non-uniform street canyon cases with the street aspect ratio $S/H = 1$.

For the step-up street canyon, the fluid flux entering into the canyon from the roof of the upwind building is larger than the previously studied uniform canyon cases, as is suggested from the figure 12(a). This is due to the fact that decrease in height of the upwind building compared to the downwind building allows more fluid to enter into the gap compare to previously studies uniform street canyon for $S/H = 1$. This high flux fluid pushes the lateral shear layers outward more as can be seen in the pathline plot representation figure 13(a) in the XZ -plane at $Y = 1$. In this case, the flow in the canyon spacing can be characterized by a strong fluid stream directed downward towards the windward face of the downwind building. The core of the recirculation vortex inside the canyon is located near the mid height of the downwind building. For the step-down canyon, a large back-flow can be seen on the roof of the downwind building as shown in figure 12(b). Since for both studied non-uniform street canyon cases, the reattachment behavior

of the separated shear layers from the leading edges of the upwind building is similar to that discussed in section 3, it is expected that the flow is bistable inside the street canyon.

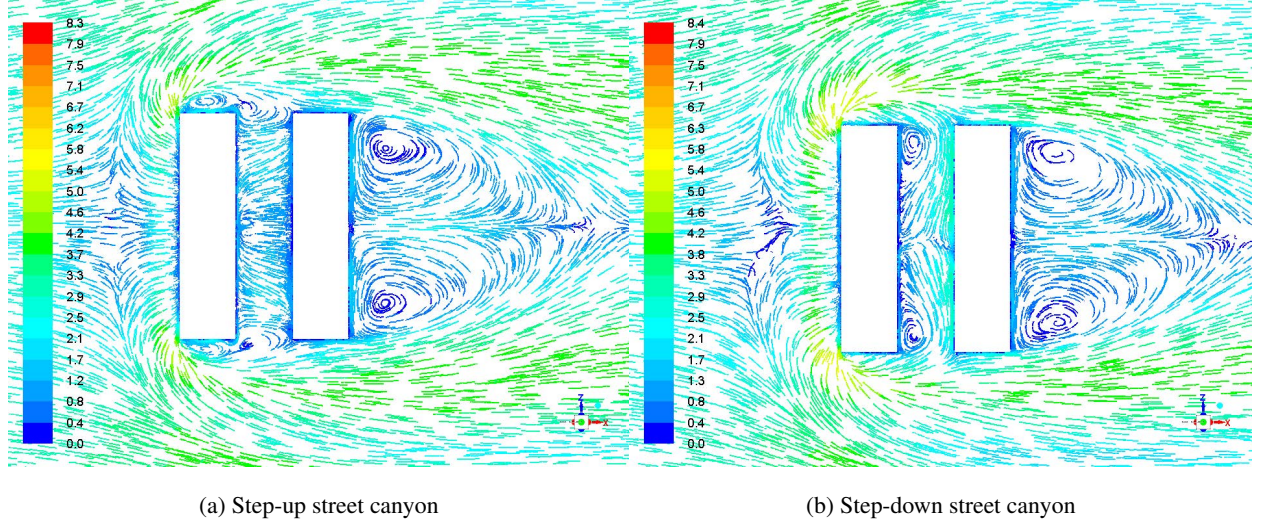


Figure 13: Velocity magnitude (m/s) pathlines in XZ- plane at $Y = 1$ m level for the non-uniform street canyon cases with the street aspect ratio $S/H = 1$.

4.2. Pedestrian comfort inside the non-uniform street canyon

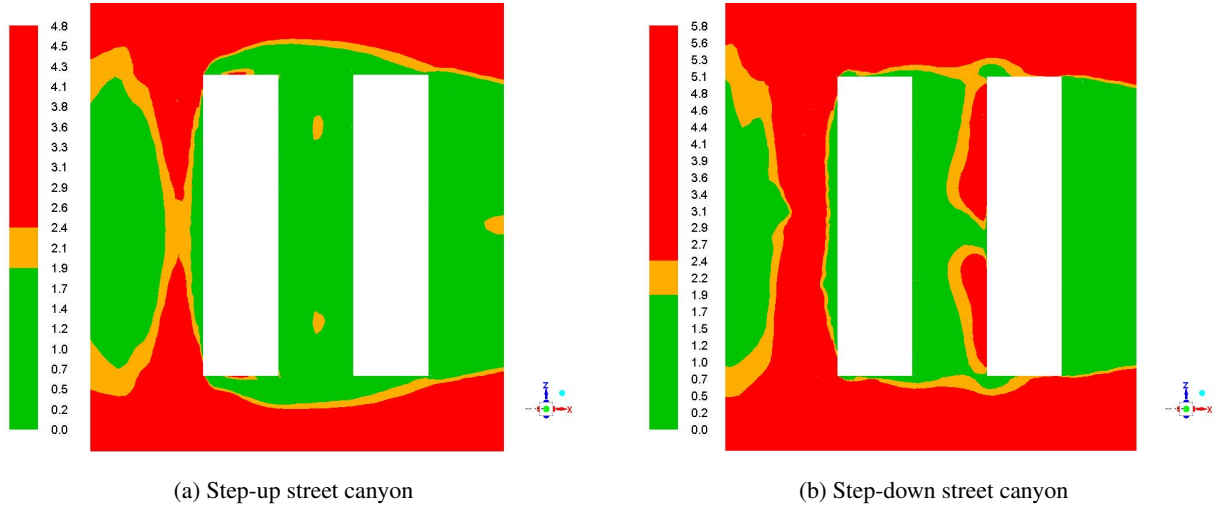


Figure 14: Velocity magnitude (m/s) contours at $Y = 1$ m in the XZ- plane for the non-uniform street canyon cases with the street aspect ratio $S/H = 1$. Here, green represents 0 to 1.8 m/s (which can be considered a comfort zone for pedestrians), orange represents 1.81 to 2.4 m/s (zone in which the wind starts causing impact on people), red represents wind speeds above 2.4 m/s (the danger zone).

Figure 14 shows contour plots of pedestrian comfort at a height of 1 m inside the street canyon for both studied non-uniform canyon cases. Almost 100% of the area inside the step-up canyon which could be in frequent use by pedestrians is in the comfort zone. Whereas for the step-down street canyon there is a region of approximately 20 – 30% of the width of the canyon which is in the danger zone.

At the pedestrian standing height, a contour plot representation for the studied non-uniform street canyon has been shown in figure 15. There is no significant difference in the pedestrian comfort at the seating height and the standing height has been observed for studied cases.

From the above studied cases it can be revealed that the pedestrian accessible zone near the upwind wall of the downwind building in uniform studied case of $S/H = 1$ which was in the danger zone can be seen in the comfort zone for the step-up street canyon at different pedestrian level height. Whereas in the case of step-down canyon drastic increase in the wind speed near the downwind building inside canyon can be seen. Therefore, it can be concluded that, a step-up street canyon is the better configuration to improve the wind speed inside the street canyon.

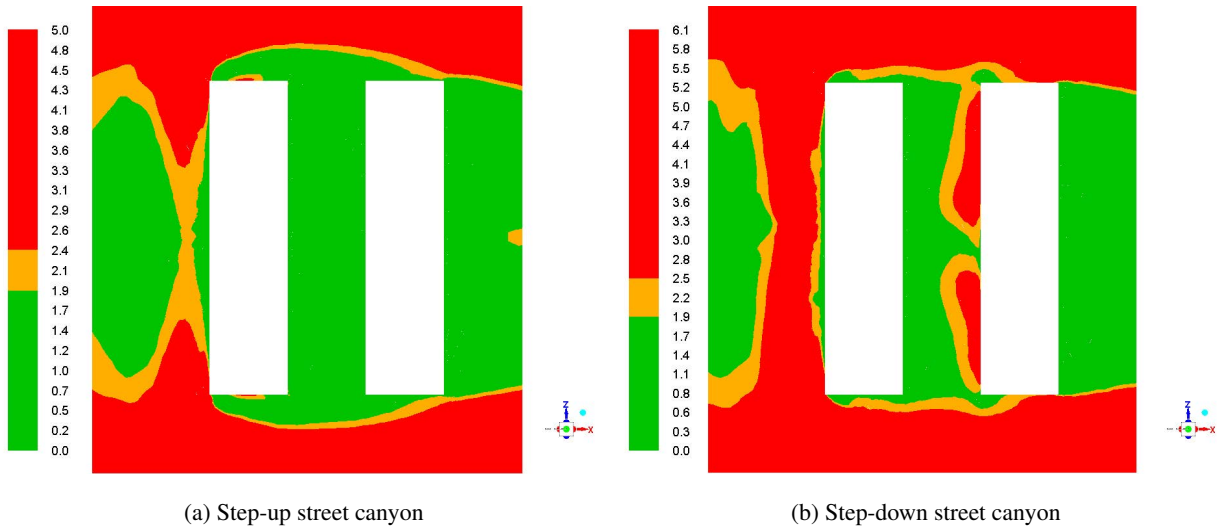


Figure 15: Velocity magnitude (m/s) contours at $Y = 1.75$ m in the XZ - plane for the non-uniform street canyon cases with the street aspect ratio $S/H = 1$. Here, green represents 0 to 1.8 m/s (which can be considered a comfort zone for pedestrians), orange represents 1.81 to 2.4 m/s (zone in which the wind starts causing impact on people), red represents wind speeds above 2.4 m/s (the danger zone).

5. Conclusion

1. In this study, the flow structure and pedestrian comfort inside uniform and non-uniform street canyons for different street-width-to-building height ratios have been analyzed using steady RANS simulations.
2. For the uniform street canyon cases, it has been observed that increase in the street width introduces more fluid flux entering into the canyon.
3. Pedestrian accessible area near the upwind building inside the canyon for all studied uniform street canyon cases is in the comfortable zone. Whereas, drastic increase in the wind speed with increase in the street width,

which causes discomfort and danger to pedestrians has been observed near the downwind building. In the case of $S/H = 1$, there is a region of approximately 20 – 30% of the width of the canyon which is in the danger zone.

4. Impact of changing the building height on the pedestrian comfort has been analyzed in the section 4 in this study. For the step-up street canyon studied case almost 100% area accessible by pedestrians is in the comfort zone. Whereas for the step-down canyon, pedestrian accessible area near the downwind building which was in the discomfort zone for the uniform street canyon case of $S/H = 1$ is in the danger zone.
5. It has been predicted in the present studied cases that vortex shedding occurs inside the canyon and in the wake of the downwind building. Transient flow simulations are required to confirm the predictions. The reason why steady RANS CFD is not capable of reproducing the vortex shedding in the wake of buildings or inside street canyons is due to the underestimation of turbulent kinetic energy in these regions [6] and that it's a steady model of an intrinsically unsteady phenomenon. Therefore, it is desirable to use unsteady RANS or Large Eddy Simulations (LES) for highly accurate CFD analysis. However, in order to use these models for predicting wind environment around buildings, a dramatic increase in computer processing speed is needed. Unsteady RANS modeling was used for validation study for the single cube case and a total of 16CPUs were used in parallel for the simulation. It takes approximately 10 days to get desired results.
6. Also note that this study considers only one wind direction, and results will vary with other wind directions.

6. Remarks

7. Appendix

7.1. Calculation for the reference wind speed

According to Blocken and Persoon [4], to assess the wind climate at a particular location requires the combination of (1) statistical meteorological data; (2) aerodynamic information and (3) a comfort criteria.

Statistical meteorological data

Generally, data are selected from a nearby meteorological station at which the wind climate is considered representative for the building site [4]. An ideal meteorological station according to Blocken and Persoon [4] is the one with aerodynamic roughness length $y_0 = 0.03$ m and gives the mean wind speed at 10 m height. In this study, we have considered the buildings or street canyon belongs to the city area of the country like New Zealand or Australia. The meteorological data at 10m height for last five years from the airport location of the city New Plymouth, New Zealand has been obtained by MetService, NZ. Analyzed cumulative mean wind speed data for the considered station is as shown in the figure 16.

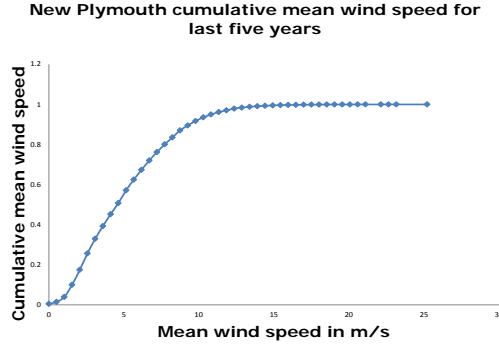


Figure 16: Cumulative mean wind speed data for New Plymouth at airport station (at height of 10 m) for last five years.

Aerodynamic information

The aerodynamic information is used to transfer the statistical meteorological data from the meteorological station to the location of interest at the building site ([4]). In this study, we have considered the terrain with roughness length $y_0 = 0.2$ according to Australian/New Zealand Standard AS/NZS 1170.2:2011 [1] (page:19) for the location of our building site. This roughness length and terrain type belongs to a woodland forest according to Davenport roughness classification table 4 from Wieringa [44] and power law wind velocity profiles for surfaces of different roughness Fig. 5 from Davenport [14]. The specified power law exponent for this type of terrain is $\alpha = 0.28$ and gradient height is $y_g = 1300' = 396.24$ m (Above the layer of frictional influence near the surface the air moves purely under the influence of the pressure gradients and attains what is know as *gradient velocity* denoted by U_g and the height above ground at which the gradient velocity is attained is generally defined as *gradient height*, denoted by y_g Davenport [14]). The meteorological station or airport station, according to above mentioned references belongs to flat open country, for which $\alpha = 0.16$ and gradient height is $y_g = 900' = 274.32$ m.

Comfort criteria

Most of the wind comfort criteria mentioned in the literature review is the combination of a wind discomfort and danger threshold. We are using extended “Land Beaufort Scale” by Lawson and Penwarden [26] as a comfort criteria for this study. As mentioned in Introduction section of this paper, we are analyzing wind velocity of $U_{1.75m} = 3$ m/s at the pedestrian height at the location of interest at the building site. Therefore according to power law wind velocity profile,

$$\frac{U_{ref}}{U_g} = \left(\frac{y_{ref}}{y_g} \right)^\alpha ;$$

and at pedestrian height

$$\frac{U_{1.75m}}{U_g} = \left(\frac{y = 1.75m}{y_g} \right)^\alpha ;$$

$$\frac{3}{U_g} = \left(\frac{1.75}{396.24} \right)^{0.28};$$

Which gives,

$$U_g = 13.7 \text{ m/s}.$$

To get real life occurrence of wind speed of 3 m/s at pedestrian height for the location of interest, we transferred the obtained wind speed in to the wind speed available at airport station of New Plymouth, New Zealand. According to Davenport [14] and Ismail [24], velocity at gradient height of different terrain types are equal, which implies that, at airport station if we consider velocity at 10 m to be U_{10m} , then using power law wind profile for corresponding profile type,

$$\frac{U_{10m}}{U_g} = \left(\frac{y = 10 \text{ m}}{y_g} \right)^\alpha;$$

where, as we considered above, substituting, $\alpha = 0.16$ and gradient height $z_g = 900' = 274.32 \text{ m}$, gives

$$\frac{U_{10m}}{13.7} = \left(\frac{y = 10 \text{ m}}{274.32} \right)^{0.16}$$

Therefore, velocity at 10 m, at airport station, will be,

$$U_{10m} = 8.1 \text{ m/s}$$

This velocity of 8.1 m/s has been occurred for approximately 17%, of the times since last five years (Figure 16). so, if we consider, the building height (H) to be 20 m, the velocity calculation at building height U_{ref} will be,

$$\frac{U_{ref}}{U_g} = \left(\frac{y = 20 \text{ m}}{396.24} \right)^{0.28}$$

Therefore,

$$U_{ref} = 5.9 \text{ m/s}$$

and Reynolds number at this height will be,

$$Re = \frac{\rho \cdot U_{ref} \cdot L}{\mu} = 8.1 \times 10^6.$$

7.2. Calculation for the boundary layer thickness

According to Counihan et al. [13], the equation to calculate boundary layer thickness is given as,

$$U(y) = U_\infty \left[\frac{(y - y_1)}{\delta} \right]^n; \quad (5)$$

Here we take, $U_\infty = 8.4$ is the wind speed outside the boundary layer (as shown in Figure 17). The exponent $n = 0.28$ and y_1 is a zero-plane displacement which is according to Garratt et al. [18] (chapter-4, page no:86) may be ignored in case of measurement are made over the short grass. Therefore equation 5 becomes;

$$U(y) = U_\infty \left[\frac{y}{\delta} \right]^n; \quad (6)$$

and calculating δ using equation 6 gives value of $\delta \approx 70$. So, $\delta/H \approx 3.5$ in present study.

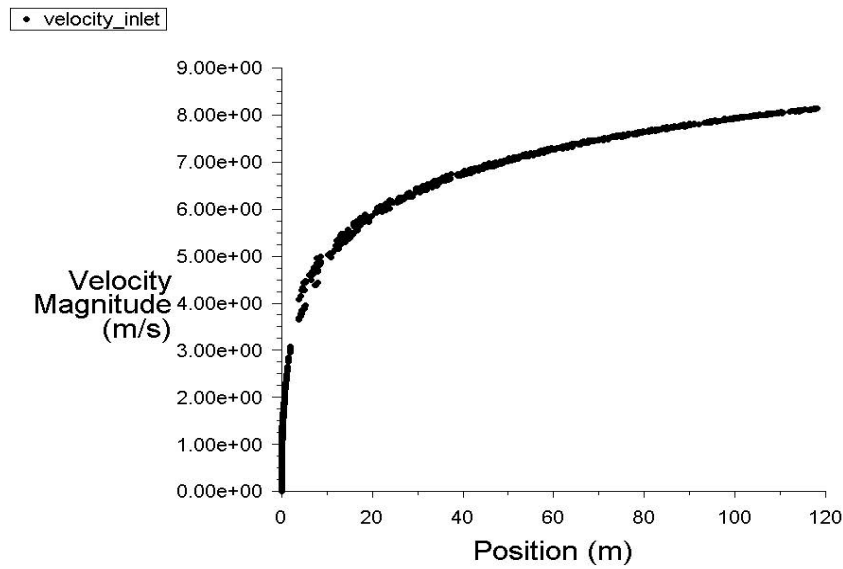


Figure 17: Boundary layer profile for the wind velocity at the inlet section of the considered uniform flow simulation cases.

References

- [1] Australian/New Zealand Standard AS/NZS 1170.2:2011. Structural design actions, Part 2: Wind actions. Standard, Standards New Zealand, Private Bag 2439, Wellington 6140, 2011.
- [2] Appupillai Baskaran and Ahmed Kashef. Investigation of air flow around buildings using computational fluid dynamics techniques. *Engineering Structures*, 18(11):861–875, 1996.
- [3] Bert Blocken and Jan Carmeliet. Pedestrian wind environment around buildings: Literature review and practical examples. *Journal of Thermal Envelope and Building Science*, 28(2):107–159, 2004.
- [4] Bert Blocken and J Persoon. Pedestrian wind comfort around a large football stadium in an urban environment: Cfd simulation, validation and application of the new dutch wind nuisance standard. *Journal of Wind Engineering and Industrial Aerodynamics*, 97(5):255–270, 2009.
- [5] Bert Blocken, Jan Carmeliet, and Ted Stathopoulos. Cfd evaluation of wind speed conditions in passages between parallel buildings: effect of wall-function roughness modifications for the atmospheric boundary layer flow. *Journal of Wind Engineering and Industrial Aerodynamics*, 95(9):941–962, 2007.
- [6] Bert Blocken, Ted Stathopoulos, Jan Carmeliet, and Jan LM Hensen. Application of computational fluid dynamics in building performance simulation for the outdoor environment: an overview. *Journal of Building Performance Simulation*, 4(2):157–184, 2011.
- [7] Marcel Bottema. Wind climate and urban geometry. *Tech. Univ. Eindhoven, Faculteit Bouwkunde, Vakgroep Fago, Rapport*, (92.63), 1992.
- [8] Marcel Bottema. A method for optimisation of wind discomfort criteria. *Building and Environment*, 35(1):1–18, 2000.
- [9] IP Castro. Measurements in shear layers separating from surface-mounted bluff bodies. *Journal of Wind Engineering and Industrial Aerodynamics*, 7(3):253–272, 1981.
- [10] IP Castro and M Dianat. Surface flow patterns on rectangular bodies in thick boundary layers. *Journal of Wind Engineering and Industrial Aerodynamics*, 11(1-3):107–119, 1983.
- [11] IP Castro and AG Robins. The flow around a surface-mounted cube in uniform and turbulent streams. *Journal of fluid Mechanics*, 79(02): 307–335, 1977.

- [12] Nicholas John Cook. Designers guide to wind loading of building structures. part 1. 1986.
- [13] J Counihan, JCR Hunt, and PS Jackson. Wakes behind two-dimensional surface obstacles in turbulent boundary layers. *Journal of Fluid Mechanics*, 64(03):529–564, 1974.
- [14] Alan G Davenport. The relationship of wind structure to wind loading. 1966.
- [15] M Dianat and IP Castro. Fluctuating surface shear stresses on bluff bodies. *Journal of wind engineering and industrial aerodynamics*, 17(1): 133–146, 1984.
- [16] M Farhadi and K Sedighi. Flow over two tandem wall-mounted cubes using large eddy simulation. *Proceedings of the Institution of Mechanical Engineers, Part C: Journal of Mechanical Engineering Science*, 222(8):1465–1475, 2008.
- [17] Jörg Franke and Alexander Baklanov. *Best practice guideline for the CFD simulation of flows in the urban environment: COST action 732 quality assurance and improvement of microscale meteorological models*. Meteorological Inst., 2007.
- [18] JR Garratt et al. The atmospheric boundary layer. cambridge atmospheric and space science series. *Cambridge University Press, Cambridge*, 416:444, 1992.
- [19] Brian Havel. *Experimental and numerical investigation of the coherent flow structures around tandem in-line surface-mounted cubes in a thin boundary layer*. 2006.
- [20] Norbert Hölscher and Hans-Jürgen Niemann. Towards quality assurance for wind tunnel tests: A comparative testing program of the windtechnologische gesellschaft. *Journal of Wind Engineering and Industrial Aerodynamics*, 74:599–608, 1998.
- [21] H J& Hussein and RJ Martinuzzi. Energy balance for turbulent flow around a surface mounted cube placed in a channel. *Physics of Fluids (1994-present)*, 8(3):764–780, 1996.
- [22] H Irtaza, RG Beale, MHR Godley, and A Jameel. Comparison of wind pressure measurements on silsoe experimental building from full-scale observation, wind-tunnel experiments and various cfd techniques. *International Journal of Engineering, Science and Technology*, 5(1):28–41, 2013.
- [23] Hatsiio Ishizaki and In Whan Sung. Influence of adjacent buildings to wind. In *Proceedings 3rd International Conference on Wind Effects on Buildings and Structures*, pages 145–152, 1971.
- [24] AM Ismail. Porosity effect in the prediction of wind-induced ventilation for the tropics.
- [25] A Larousse, R Martinuzzi, and C Tropea. Flow around surface-mounted, three-dimensional obstacles. In *Turbulent Shear Flows 8*, pages 127–139. Springer, 1993.
- [26] TV Lawson and AD Penwarden. The effects of wind on people in the vicinity of buildings. In *Proceedings 4th International Conference on Wind Effects on Buildings and Structures, Cambridge University Press, Heathrow*, pages 605–622, 1975.
- [27] R Martinuzzi and C Tropea. The flow around surface-mounted, prismatic obstacles placed in a fully developed channel flow (data bank contribution). *Journal of Fluids Engineering*, 115(1):85–92, 1993.
- [28] R Martinuzzi and C Tropea. The flow around surface-mounted, prismatic obstacles placed in a fully developed channel flow (data bank contribution). *Journal of Fluids Engineering*, 115(1):85–92, 1993.
- [29] Robert J Martinuzzi and Brian Havel. Turbulent flow around two interfering surface-mounted cubic obstacles in tandem arrangement. *Journal of fluids engineering*, 122(1):24–31, 2000.
- [30] Robert J Martinuzzi and Brian Havel. Turbulent flow around two interfering surface-mounted cubic obstacles in tandem arrangement. *Journal of fluids engineering*, 122(1):24–31, 2000.
- [31] Robert J Martinuzzi and Brian Havel. Vortex shedding from two surface-mounted cubes in tandem. *International journal of heat and fluid flow*, 25(3):364–372, 2004.
- [32] ER Meinders and K Hanjalić. Vortex structure and heat transfer in turbulent flow over a wall-mounted matrix of cubes. *International Journal of Heat and Fluid Flow*, 20(3):255–267, 1999.
- [33] Joongcheol Paik, Fotis Sotiropoulos, and Fernando Porté-Agel. Detached eddy simulation of flow around two wall-mounted cubes in tandem. *International Journal of Heat and Fluid Flow*, 30(2):286–305, 2009.
- [34] G Seeta Ratnam and S Vengadesan. Performance of two equation turbulence models for prediction of flow and heat transfer over a wall

- mounted cube. *International Journal of Heat and Mass Transfer*, 51(11):2834–2846, 2008.
- [35] PJ Richards and RP Hoxey. Flow reattachment on the roof of a 6m cube. *Journal of Wind Engineering and Industrial Aerodynamics*, 94(2): 77–99, 2006.
 - [36] PJ Richards, RP Hoxey, and LJ Short. Wind pressures on a 6m cube. *Journal of Wind Engineering and Industrial Aerodynamics*, 89(14): 1553–1564, 2001.
 - [37] PJ Richards, RP Hoxey, BD Connell, and DP Lander. Wind-tunnel modelling of the silsoe cube. *Journal of Wind Engineering and Industrial Aerodynamics*, 95(9):1384–1399, 2007.
 - [38] W Rodi. Comparison of les and rans calculations of the flow around bluff bodies. *Journal of wind engineering and industrial aerodynamics*, 69:55–75, 1997.
 - [39] Hy Sakamoto and H Haniu. Aerodynamic forces acting on two square prisms placed vertically in a turbulent boundary layer. *Journal of Wind Engineering and Industrial Aerodynamics*, 31(1):41–66, 1988.
 - [40] WH Schofield and E Logan. Turbulent shear flow over surface mounted obstacles. *Journal of fluids engineering*, 112(4):376–385, 1990.
 - [41] Kishan B Shah and Joel H Ferziger. A fluid mechanics view of wind engineering: Large eddy simulation of flow past a cubic obstacle. *Journal of Wind Engineering and Industrial Aerodynamics*, 67:211–224, 1997.
 - [42] AP To and KM Lam. Evaluation of pedestrian-level wind environment around a row of tall buildings using a quartile-level wind speed descriptor. *Journal of wind engineering and industrial aerodynamics*, 54:527–541, 1995.
 - [43] Sotiris Vardoulakis, Reneta Dimitrova, Kate Richards, David Hamlyn, Giorgio Camilleri, Mark Weeks, Jean-François Sini, Rex Britter, Carlos Borrego, Michael Schatzmann, et al. Numerical model inter-comparison for wind flow and turbulence around single-block buildings. *Environmental Modeling & Assessment*, 16(2):169–181, 2011.
 - [44] Jon Wieringa. Updating the davenport roughness classification. *Journal of Wind Engineering and Industrial Aerodynamics*, 41(1):357–368, 1992.
 - [45] BG Wiren. A wind tunnel study of wind velocities in passages between and through buildings. In *Proceedings of the 4th International Conference on Wind Effects on Buildings and Structures,(Heathrow 1975)*, pages 465–475, 1975.
 - [46] Tong Yang. *CFD and field testing of a naturally ventilated full-scale building*. PhD thesis, University of Nottingham, 2004.